JPEDAV (2016) 37:277–292
DOI: 10.1007/s11669-016-0454-2
1547-7037 ©ASM International

Thermodynamic Assessment of the Fe-Ca-S, Fe-Mg-O and Fe-Mg-S Systems

David Dilner, Lina Kjellqvist, and Malin Selleby

(Submitted December 2, 2015; in revised form February 5, 2016; published online February 18, 2016)

Thermodynamic descriptions of the Fe-Mg-O, Fe-Ca-S and Fe-Mg-S systems are all important in order to perform thermodynamic calculations related to the steelmaking process. The experimental information of many sulphur-containing systems, including Fe-Ca-S and Fe-Mg-S, is lacking and they are here thus approximated to behave similarly to the corresponding oxygen systems. This study presents a description of the Fe-Mg-O system in good agreement with experimental information. Additionally, descriptions of the Fe-Ca-S and Fe-Mg-S systems are presented. These descriptions may be reasonable estimations considering the lack of experimental information.

Keywords CALPHAD, equilibria, Fe-Ca-S, Fe-Mg-O, Fe-Mg-S, ionic two-sublattice liquid model, steelmaking

1. Introduction

Calcium and magnesium are two elements of great importance for the steelmaking process. Calcium oxide (lime) is one of the main components in many slags. Additionally, calcium additions are the most common additives for sulphur refining. Ladle walls are often made of magnesium oxide (magnesia) bricks. Since calcium and magnesium belong to the same group in the periodic table they have quite similar chemical properties, including the same oxidation number in compounds and similar electronegativity. The main differences between them are their ionic radii and their atomic weights. Due to their importance in the steelmaking process it is vital to have thermodynamic descriptions containing these elements together with iron, oxygen and sulphur. The Fe-Ca-O system has been assessed previously[1,2] using the ionic two-sublattice model.[3,4] But two of the ternary systems are missing, i.e. the Fe-Ca-S and Fe-Mg-S systems. The Fe-Mg-O system has been assessed by both Fabrichnaya[5] and Jung et al.,[6] but is reassessed in this work. Fabrichnaya's assessment[5] is mainly concerned phase equilibria at high pressures. A simplified model for the spinel phase was adopted and the liquid phase was excluded. Jung et al.[6] assessed the Fe-Mg-O system using the modified quasi-chemical model[7] for the liquid phase. No assessments have been reported previously for the Fe-Ca-S or Fe-Mg-S systems. However, the Ca-S system has been assessed previously, as a part of the Ca-O-S-C system[8] using the modified quasi-chemical mode.

Parameters were taken from existing assessments of the Fe-Ca,[2] Fe-Mg,[9] Fe-S,[10] Ca-O,[2] Fe-O[11] and Mg-O[12] systems, respectively. Due to lack of experimental data concerning the Ca-S and Mg-S systems the liquid parameters from the corresponding oxide systems Ca-O[2] and Mg-O[12] are used. The aim of this study is to obtain databases for phases in the Fe-Mg-O, Fe-Ca-S and Fe-Mg-S systems in order to describe experimental data at atmospheric pressure using the compound energy formalism (CEF) to describe the solid phases and the ionic two-sublattice liquid (i2sl) model for the liquid metal and slag. The principal phases in the Fe-Mg-O system are liquid, solid iron (bcc, fcc), solid magnesium (hcp), halite ($Fe_{1-x}Mg_xO$, $0 < x < 1$), spinel ($Fe_{3-x}Mg_xO_4$, $0 < x < 1$) and corundum (Fe_2O_3). In the Fe-Ca-S and Fe-Mg-S systems the principal phases are liquid, iron (bcc, fcc), magnesium (hcp), calcium (bcc, fcc), alabandite (Ca, Fe, Mg)S and pyrrhotite ($Fe_{1-x}S$).

2. Thermodynamic Models

In this assessment the systems are described using the CALPHAD-method.[13] All solution phases are modelled using the compound energy formalism.[14,15]

2.1 Liquid

As mentioned in the introduction, the liquid phase is modelled using the ionic two-sublattice model.[4,14] This model can describe the metallic liquid, the ionic liquid, and in the case of sulphur systems the liquid sulphur. In general the ionic two-sublattice model can be represented as:

$$(C_i^{v_i})_P\left(A_j^{v_j}, \mathrm{Va}^{-Q}, B_k^0\right)_Q$$

where C denotes cations, A anions, Va vacancies, B neutral species and v charge. P and Q are variable size of the

David Dilner and **Malin Selleby,** Materials Science and Engineering, KTH Royal Institute of Technology, Brinellvägen 23, 100 44 Stockholm, Sweden; **Lina Kjellqvist,** Thermo-Calc Software AB, Norra Stationsgatan 93, 113 64 Stockholm, Sweden. Contact e-mail: dilner@kth.se.

sublattices to maintain electroneutrality. The molar Gibbs energy in the general case can be described as:

$$G_{\mathrm{m}} = \sum_i \sum_j y_{C_i} y^{\circ}_{A_j} G_{C_i:A_j} + Q y_{\mathrm{Va}} \sum_i y^{\circ}_{C_i} G_{C_i} + Q \sum_k y^{\circ}_{B_k} G_{B_k} + RT\left(P \sum_i y_{C_i} \ln y_{C_i} + Q\left(\sum_j y_{A_j} \ln y_{A_j} + y_{\mathrm{Va}} \ln y_{\mathrm{Va}} + \sum_k y_{B_k} \ln y_{B_k} \right) \right) + {}^{E}G_{\mathrm{m}}$$

where ${}^{\circ}G_{C_i:A_j}$ denotes the Gibbs energy of pure ionic liquids, ${}^{\circ}G_{C_i}$ the Gibbs energy of pure metallic liquids, ${}^{\circ}G_{B_k}$ pure neutral liquids, e.g. liquid sulphur, and ${}^{E}G_{\mathrm{m}}$ denotes the molar excess Gibbs energy. y_{C_i}, y_{A_j}, y_{Va} and y_{B_k} represent the site fractions of cations, anions, vacancies and neutrals respectively. The binary part of the excess energy is given by:

$$\begin{aligned} {}^{E}G = & \sum_i \sum_{i_2 > i_1} \sum_k y_{C_{i_1}} y_{C_{i_2}} y_{A_j} L_{C_{i_1},C_{i_2}:A_j} \\ & + \sum_i \sum_{j_1} \sum_{j_2 > j_1} y_{C_i} y_{A_{j_1}} y_{A_{j_2}} L_{C_i:A_{j_1},A_{j_2}} \\ & + \sum_i \sum_j \sum_k y_{C_i} y_{A_j} y_{B_k} L_{C_i:A_j,B_k} \\ & + y_{\mathrm{Va}} \sum_i \sum_j y_{C_i} y_{A_j} L_{C_i:A_j,\mathrm{Va}} \\ & + Q y_{\mathrm{Va}} \sum_i \sum_{i_2 > i_1} y_{C_{i_1}} y_{C_{i_2}} L_{C_{i_1},C_{i_2}:\mathrm{Va}} \\ & + Q y_{\mathrm{Va}} \sum_i \sum_k y_{C_i} y_{B_k} L_{C_i:\mathrm{Va},B_k} \\ & + Q \sum_{k_1} \sum_{k_2 > i_1} y_{B_{k_1}} y_{B_{k_2}} L_{B_{k_1},B_{k_2}} \end{aligned}$$

where the different L are the different interaction parameters. For example $L_{C_{i_1},C_{i_2}:\mathrm{Va}}$ is the interaction parameter for two cations with vacancies on the second sublattice, i.e. mixing of two metallic atoms. In addition to these binary interaction parameters some reciprocal parameters or ternary interaction parameters may be needed in some systems.

2.2 Halite and Alabandite

The monoxides, CaO and MgO, as well as the monosulphides, CaS and MgS,[16] all have a NaCl structure. It is known that all NaCl-monoxides of importance for steelmaking, including FeO and MnO, are strongly ionic. However, for sulphides this is not always the case, for example with MnS, which is a semiconductor with a bandgap of about 3 eV.[17] The solubility of oxygen and sulphur in the sulphides and oxides respectively is reported to be very low, as in the MnO-MnS system [18] or unknown. Due to this the monoxides and monosulphide with the NaCl-structure are treated as two separate phases. The notation is halite for the oxide phase and alabandite for the sulphide phase, to be consistent with previous descriptions of oxides, see e.g., Ref 1, 2, 19-22 and sulphides.[23] It is known that the halite exhibits some non-stoichiometry with respect to oxygen when it dissolves Fe[11] and Mn.[24] The non-stoichiometry in MnS is very low[25] which is likely the case also for CaS, MgS and metastable [NaCl]-FeS.

$$\text{Halite: } \left(\mathrm{Fe}^{+2}, \mathrm{Fe}^{+3}, \mathrm{Ca}^{+2}, \mathrm{Mg}^{+2}, \mathrm{Va}\right)\left(\mathrm{O}^{-2}\right)$$

$$\text{Alabandite: } (\mathrm{Ca}, \mathrm{Mg}, \mathrm{Fe})\mathrm{S}$$

2.3 Spinel

The spinel phase consists of magnetite (Fe_3O_4) and magnesioferrite ($MgFe_2O_4$). In the stoichiometric spinel structure, cations occupy tetrahedral (first sublattice) and octahedral (second sublattice) sites, while the oxygen ions form an fcc lattice (last sublattice). Depending on the distribution of cations between tetrahedral and octahedral sites, the spinel structure can be normal or inverse. In the normal spinel structure, divalent ions occupy tetrahedral sites and trivalent ions octahedral sites. If the tetrahedral sites are occupied with trivalent ions, the spinel is referred to as inverse. A common way to express the degree of inversion is to give the site fraction of trivalent ions on the tetrahedral sublattice. At low temperatures, both magnetite and magnesioferrite are inverse spinels with Fe^{+3} on the tetrahedral sites. At higher temperatures, the degree of inversion decreases. The model for the stoichiometric spinel is thus:

$$\left(\mathrm{Fe}^{+2}, \mathrm{Fe}^{+3}, \mathrm{Mg}^{+2}\right)_1\left(\mathrm{Fe}^{+2}, \mathrm{Fe}^{+3}, \mathrm{Mg}^{+2}\right)_2\left(\mathrm{O}^{-2}\right)_4$$

The spinel phase can deviate from its stoichiometry both toward excess metal and excess oxygen. Fe^{+3} is introduced into the octahedral sublattice to model the deviation towards higher oxygen potentials. Vacancies are formed to maintain electroneutrality:

$$\left(\mathrm{Fe}^{+2}, \mathrm{Fe}^{+3}, \mathrm{Mg}^{+2}\right)_1\left(\mathrm{Fe}^{+2}, \mathrm{Fe}^{+3}, \mathrm{Mg}^{+2}, \mathrm{Va}\right)_2\left(\mathrm{O}^{-2}\right)_4$$

To model the deviation towards excess metal, Fe^{+2} and Mg^{+2} are introduced as interstitials on an extra octahedral site which is normally empty:

$$\left(\mathrm{Fe}^{+2}, \mathrm{Fe}^{+3}, \mathrm{Mg}^{+2}\right)_1\left(\mathrm{Fe}^{+2}, \mathrm{Fe}^{+3}, \mathrm{Mg}^{+2}, \mathrm{Va}\right)_2 \left(\mathrm{Fe}^{+2}, \mathrm{Mg}^{+2}, \mathrm{Va}\right)_2\left(\mathrm{O}^{-2}\right)_4$$

Thirty-six combinations are possible, and each of the 36 compounds is given a Gibbs energy value. In practice, the number of independent parameters is smaller, since most of these end-members have a net charge and can be present only in neutral combinations. Of the 36 parameters, 12 were fixed during the Fe-O assessment,[11] and 4 were fixed in the Al_2O_3-MgO assessment.[26] The 20 remaining parameters were derived in the present study. Only 3 parameters are assessed, the remaining parameters are obtained through reciprocal reactions. Detailed descriptions of modelling of the spinel phase have been given in previous work.[19,21,27] The magnetic transition of the spinel phase is given by the model from Inden[28] and Hillert and Jarl.[29]

2.4 Corundum

The corundum phase represents the mineral hematite, Fe_2O_3, in the Fe-O system. Corundum can dissolve vacancies on some metallic sites giving rise to a small under-stoichiometry. Corundum is described by $(Fe^{+2},Fe^{+3})_2(Fe^{+3},Va)_1(O^{-2})_3$ as in the assessment of the Cr-Fe-Ni-O system.[19]

2.5 Pyrrhotite

The pyrrhotite ($Fe_{1-x}S$) phase has a NiAs structure. The description of this phase is adopted from.[10] Solubility of Ca and Mg in pyrrhotite is assumed to be very low as no solubility data have been reported.[30,31] The non-stoichiometry is treated with vacancies on the metal sublattice: (Fe,Va)S.

2.6 Metal phases

Steels have either a bcc or fcc structure depending on temperature and composition. Calcium has a bcc structure at higher temperatures and a fcc structure at low temperature. Magnesium has an hcp structure. In general the metallic phases can be described as:

$$(\mathrm{Ca,Fe,Mg,S})_1(\mathrm{O,Va})_b$$

The value of b is 3 for bcc, 1 for fcc and 0.5 for hcp. Sulphur is assumed to be dissolved substitutionally as in the Fe-S descriptions[10]which is used in this work as well as the Fe-Mn-S description.[23] Oxygen is assumed to dissolve interstitially as in.[11] The sulphur solubility in all phases with pure Ca and Mg is assumed to be very low.

2.7 Optimization

The optimization was performed using the Parrot module in the Thermo-Calc software.[32] Comparisons will be made with all experimental studies mentioned, but not all were used in the assessment. In the optimization of the compounds $MgFe_2O_4$, CaS and MgS no attempts were made to fit the low-temperature C_P data, instead the Neumann-Kopp approximation was used in the present work.

When optimizing the spinel phase, a parameter describing stoichiometric $MgFe_2O_4$ was first determined using thermochemical data, where low weight was given to the enthalpy of formation and Gibbs energy of formation. The magnetic transition temperature was fixed to the experimental value 690 K, and the Bohr magneton number was used as an optimizing parameter to fit the shape of the lambda transition. The degree of order was then used to evaluate the ordering of Fe^{+3} and Mg^{+2} on the octahedral and tetrahedral sublattices. The FeO-MgO and Fe_2O_3-MgO interactions in the halite phase are assessed in a first step mainly using oxygen isobars in the halite single-phase region. When the solid oxides in the Fe-Mg-O system had been roughly evaluated, all parameters were included in the optimization, also involving experimental information on invariant equilibria and measured oxygen potentials in the two-phase regions. After the solid oxides had been determined, the liquid phase was assessed using data on the phase boundaries between liquid oxide and halite in the iron-saturated section and the invariant temperature in air.

In the Fe-Ca-S and Fe-Mg-S systems, solid CaS and MgS, i.e. the alabandite phases, were evaluated using thermochemical data. Liquid CaS and MgS were described using Neumann-Kopp. Since no heat of fusion data is found, the melting entropy from MgO is used for both sulphides. The reason assuming that all the sulphides and oxides in this study have the same melting entropy is that this value contains the entropy difference between a strongly ionic NaCl-crystal and a strongly ionic liquid. The interaction parameters in the FeS-CaS and FeS-MgS pseudobinary systems are optimized starting with interaction parameters of the alabandite phase. The liquid interaction parameters are optimized as the alabandite parameters have been fixed. The optimized parameters for Fe-Mg-O, Fe-Ca-S and Fe-Mg-S are found in Tables 1, 2, and 3 respectively and functions are found in Table 4.

3. Result and Discussion

3.1 Fe-Mg-O

Many experimental investigations have been reported in the Fe-Mg-O system. There are mainly three types of experimental information: thermochemical and structural data for the spinel phase, non-stoichiometry of the halite phase and the phase equilibria Fe-halite, halite-spinel and spinel-corundum at different oxygen potentials.

3.2 Spinel ($Fe_{3-x}Mg_xO_4$, $0 < x < 1$)

3.2.1 Heat Capacity, Heat Content and Entropy. The heat capacity has been measured by King[33] up to 300 K and at ambient temperature by Reznitskii et al.[34] The two sets of measurements disagree as the values measured by Reznitskii et al. are considerably higher than those reported by King.[33] The magnetic transition of $MgFe_2O_4$ is observed at around 650 K according to Reznitskii et al.[34] The heat content of $MgFe_2O_4$ has been experimentally determined by Bonnickson[35] and the entropy of $MgFe_2O_4$ at 298 K is reported by King.[33] The calculated heat capacity and entropy at 298 K is 143.8 and 115.1 J/mol/K respectively compared with 143.7 and 118.4 J/mol/K, as reported by King.[33] The calculated heat content is shown in Fig. 1a together with the experimental data from Bonnickson.[35]

3.2.2 Enthalpies of Formation. The enthalpy of formation of $MgFe_2O_4$ from MgO and Fe_2O_3 have been discussed in some studies.[36-40] Navrotsky and Kleppa[40] reports the heat of formation to be -15.5 ± 1.0 kJ/mol at 970 K. According to them this is in good agreement with Tretjakow and Schmalzried[38] who estimated the heat of formation to −24.1 ± 1.7 kJ/mol at 1273 K and −20.1 ± 1.7 kJ/mol at 298 K from the temperature dependence of EMF data. However, Shearer and Kleppa[36] make a correction of 11.7 kJ/mol to the data by Navrotsky and Kleppa[40] as they use an incorrect value of the enthalpy of solution of MgO in lead-cadmium-borate, which gives −6.7 ± 2.1 kJ/mol at 970 K. This agrees reasonably well with Koehler et al.[37] who reports the heat of formation to be −2.6 ± 1.5 kJ/mol at 298 K. The calculated heat of formation at 970 K is

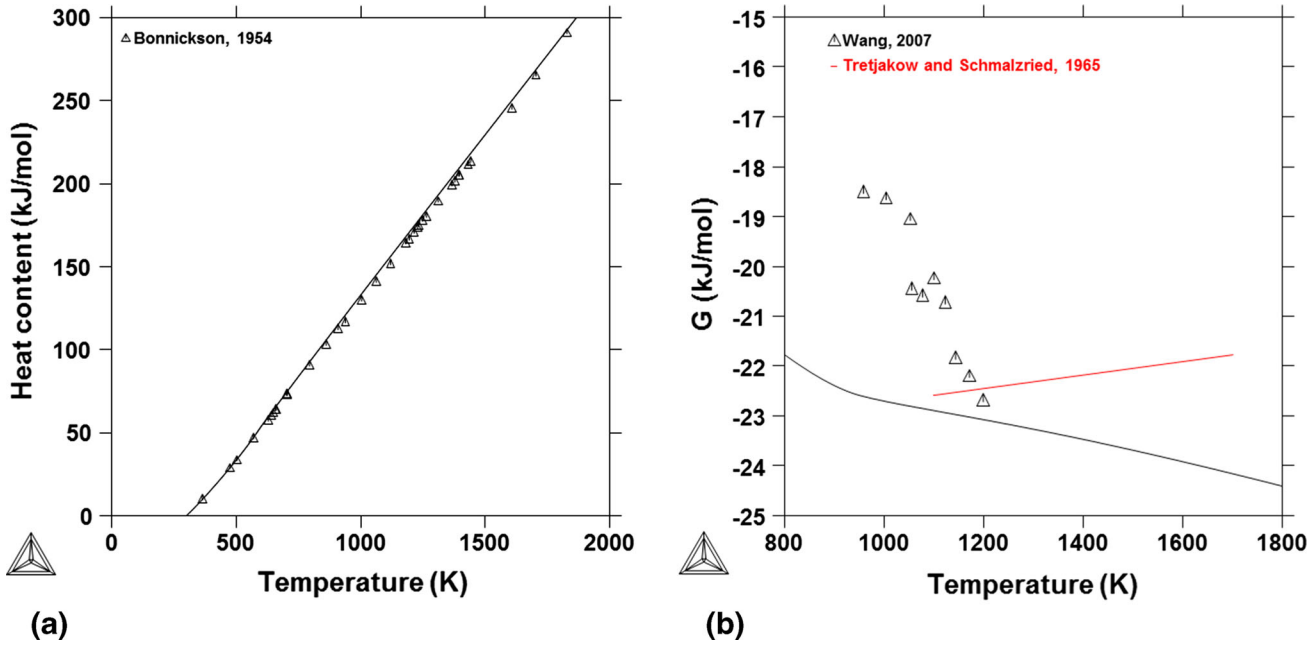

Fig. 1 Calculated (a) heat content and (b) Gibbs energy of formation for the $MgFe_2O_4$-spinel, using MgO (halite) and Fe_2O_3 (corundum) as references, together with experimental data[35,41]

−20.3 kJ/mol. A further complication regarding thermochemical data of spinels is due to uncertainties regarding the cation equilibration, as is discussed in Navrotsky.[39]

3.2.3 Gibbs Energy of Formation. Tretjakow and Schmalzried[38] determined the Gibbs energy change of $MgFe_2O_4$ relative to the component oxides using a CaO-ZrO_2 solid state electrolyte cell. They employed an air reference electrode and $MgFe_2O_4$ + MgO + Fe as the working electrode in their cells and report the Gibbs energy of formation to be −24.06 + 0.00134 T kJ/mol in the temperature range 1100 to 1700 K. Wang et al.[41] determined the Gibbs energy of $MgFe_2O_4$ relative to component oxides using a solid state cell incorporating $MgZr_4(PO_4)_6$ and a single crystal of CaF_2 as solid electrolytes. The reversible EMF of a solid state cell was measured as a function of temperature in the range 950 to 1200 K. Low weight was given the Gibbs energy of formation data in the assessment procedure. In Fig. 1a and b the heat content and Gibbs energy of formation of the spinel phase is plotted together with experimental data.

3.2.4 Structural Data. $MgFe_2O_4$ is known to be an almost inverse spinel at room temperature with Fe^{+3} on tetrahedral sites and Mg^{+2} and Fe^{+3} on octahedral sites. With increasing temperature it changes gradually into a more normal structure.[42-48] At low temperatures, the cation distribution does not have time to reach equilibrium. On the other hand, at high temperatures, it is difficult to retain the equilibrium distribution of cations on quenching. Trestman-Matts et al.[49] and Nell et al.[50] measured the degree of inversion in the $Mg_{1-x}Fe_{2+x}O_4$ spinel solution at 1000 °C. O'Neill et al.[42] report the ordering of Fe^{+3} and Mg^{+2} on the octahedral and tetrahedral sublattices. In Fig. 2 the calculated degree of inversion as function of temperature in the $MgFe_2O_4$ spinel is plotted together with experimental data.

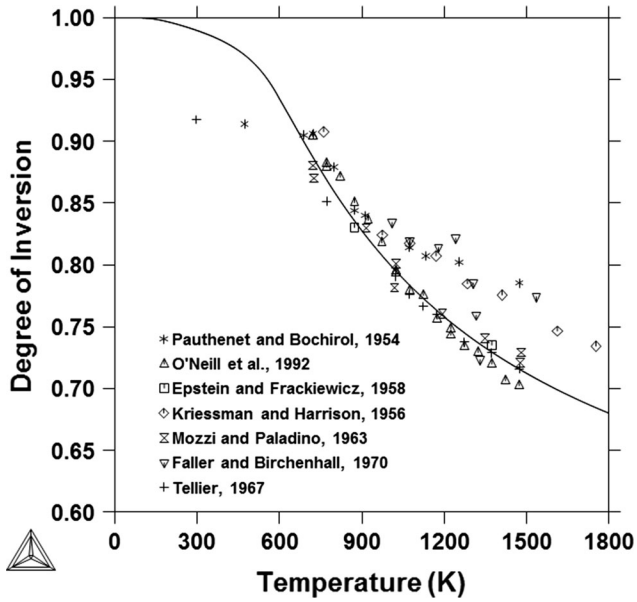

Fig. 2 Calculated degree of inversion of $MgFe_2O_4$-spinel with experimental data from[42-48]

3.3 Halite $Fe_{1-x}Mn_xO$, $0 < x < 1$

3.3.1 Non-stoichiometry. Experimental data on the non-stoichiometry of halite are quite scattered. Several investigators[51-53] have reported the Fe^{+3} content as function of composition. The calculated molar ratio $n_{Fe^{+3}}/n_{O^{-2}}$ in the halite phase in equilibrium with iron is shown in

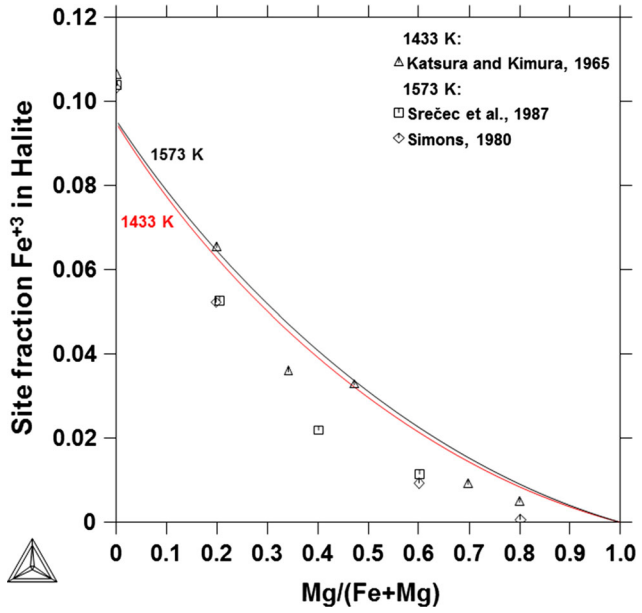

Fig. 3 Calculated cation distribution in halite as function of Fe/(Fe + Mg) in equilibrium with iron at 1433 and 1573 K with experimental data from[51-53]

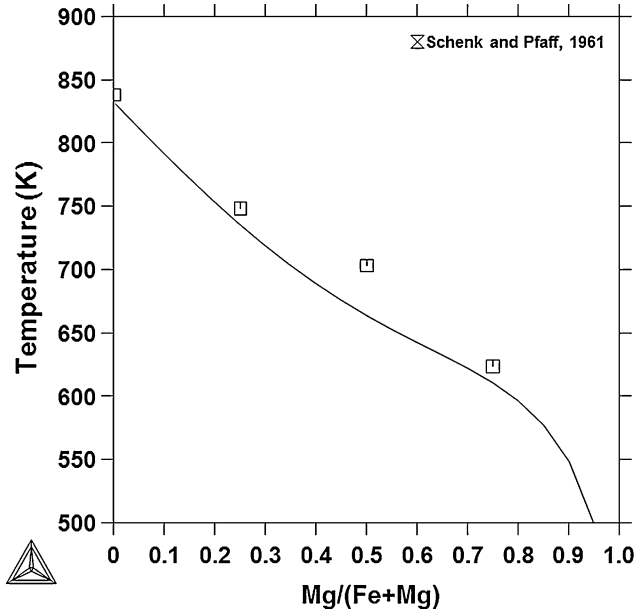

Fig. 4 Calculated dissociation temperature of halite as function of Fe/(Fe + Mg) together with experimental data[71]

Fig. 3 together with experimental data. As can be seen in the figure only a slight temperature dependence is found, both experimentally and in the calculations. The calculated values are within the experimental scatter. It was found that it was not possible to decrease the $n_{Fe^{+3}}/n_{O^{-2}}$ ratio and simultaneously fit the log (PO_2) isobars in the halite single-phase region and the halite + spinel two-phase regions without using very large ternary interaction parameters in the halite phase.

3.3.2 Phase Diagram. Halite solid solutions in equilibrium with iron were studied at different temperatures and oxygen partial pressures by several authors.[51,54-58] These data show how the total Fe and Fe^{+3} contents in halite depend on oxygen partial pressure and temperature. The phase diagram (spinel-corundum, halite-spinel, Fe-halite equilibria) of the Fe-Mg-O system at various oxygen partial pressures for temperatures between 800 and 1600 °C was studied by many authors.[38,51,54,56,58-68] Halite decomposes into Fe + spinel below about 564 °C in the binary Fe-O system. This dissociation occurs also in the ternary system, and was measured by Schmahl et al.[69] The calculated dissociation temperature is shown in Fig. 4.

MgO-Fe_2O_3. The phase diagram in air has been investigated by several authors[59,60,70] from 800 to 1750 °C. The calculated phase diagram in air is shown in Fig. 5. The true binary system MgO-Fe_2O_3 can be calculated by inserting a very high oxygen potential which is also shown in Fig. 5.

FeO-MgO with Excess Iron. The iron-saturated region ("FeO"-MgO), where the iron oxide consists mainly of FeO, was studied by many authors.[71-75] Solidus temperatures were measured by Schenck and Pfaff.[71] Liquidus

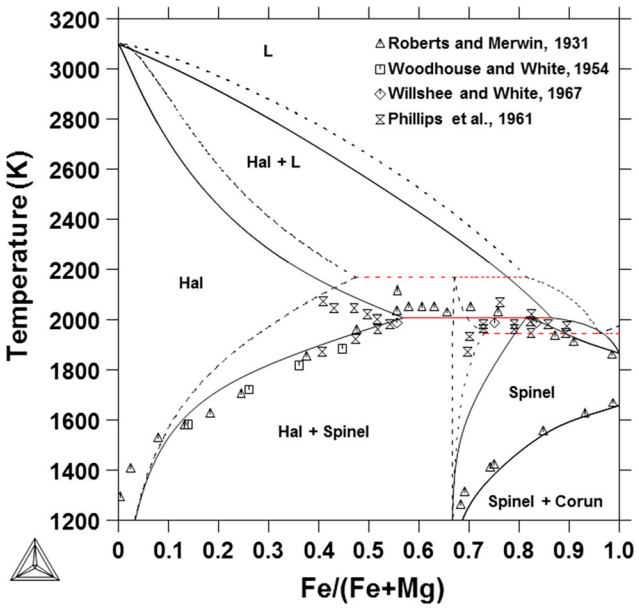

Fig. 5 Calculated pseudobinary MgO-"Fe_2O_3" phase diagram in air (a_{O2} = 0.21) with experimental phase boundary data.[59,60,70,97] The dashed line is the MgO-Fe_2O_3 phase pseudobinary calculated by setting a very high oxygen activity

temperatures were measured by several authors,[72-75] but the results are rather scattered. Metallic iron is always present, in different modifications depending on the temperature. The calculated phase diagram with excess iron is shown with experimental data[71-75] in Fig. 6. The experimental solidus temperatures are reasonably well described

Table 1 List of assessed parameters in the Fe-Mg-O system for phases that have been assessed in this work

Liquid
$G_{Fe^{+2}:Va}$ = +GFELIQ[98]
$G_{Mg^{+2}:Va}$ = +GLIQMG[98]
$G_{Fe^{+2}:O^{-2}}$ = +4GFEOLIQ[11]
$G_{Mg^{+2}:O^{-2}}$ = +2GMGOLIQ[98]
$G_{FeO^{3/2}}$ = +2.5GFEOLIQ-89819 + 39.962T[11]
$L^0_{Fe^{+2},Mg^{+2}:Va}$ = +61343 + 1.5T[9]
$L^1_{Fe^{+2},Mg^{+2}:Va}$ = −2700[9]
$L_{Fe^{+2},Mg^{+2}:O^{-2}}$ = − 20000[*]
$L^0_{Fe^{+2}:O^{-2},Va}$ = +176681 − 16.368T[11]
$L^1_{Fe^{+2}:O^{-2},Va}$ = −65655 + 30.869T[11]
$L^0_{Fe^{+2}:O^{-2},FeO^{3/2}}$ = −26362[11]
$L^1_{Fe^{+2}:O^{-2},FeO^{3/2}}$ = +13353[11]
$L_{Mg^{+2}:O^{-2},Va}$ = +182000 + 26.8T[12]
$L_{Fe^{+2}:Va,FeO^{3/2}}$ = +110000[2]
Halite
$G_{Fe^{+2}:O^{-2}}$ = +GWUSTITE[11]
$G_{Fe^{+3}:O^{-2}}$ = +1.25AWUSTITE + 1.25GWUSTITE[11]
$G_{Mg^{+2}:O^{-2}}$ = +GMGOSOL[99]
$L^0_{Fe^{+2},Fe^{+3}:O^{-2}}$ = −12324[11]
$L^1_{Fe^{+2},Fe^{+3}:O^{-2}}$ = +20070[11]
$L^0_{Fe^{+2},Mg^{+2}:O^{-2}}$ = +5200[*]
$L^1_{Fe^{+2},Mg^{+2}:O^{-2}}$ = -2000[*]
$L^0_{Fe^{+3},Mg^{+2}:O^{-2}}$ = +24000[*]
$L^1_{Fe^{+3},Mg^{+2}:O^{-2}}$ = -6800[*]
Spinel
$G_{Fe^{+2}:Fe^{+2}:Va:O^{-2}}$ = +7GFE3O4 + BFE3O4[11]
$G_{Fe^{+3}:Fe^{+2}:Va:O^{-2}}$ = +7GFE3O4[11]
$G_{Fe^{+2}:Fe^{+3}:Va:O^{-2}}$ = +7GFE3O4[11]
$G_{Fe^{+3}:Fe^{+3}:Va:O^{-2}}$ = +7GFE3O4 − BFE3O4[11]
$G_{Fe^{+2}:Va:Va:O^{-2}}$ = +5GFE3O4 + CFE3O4[11]
$G_{Fe^{+3}:Va:Va:O^{-2}}$ = +5GFE3O4 + CFE3O4 − BFE3O4[11]
$G_{Mg^{+2}:Mg^{+2}:Va:O^{-2}}$ = +NSPINEL + 2ISPINEL + 4RTln(2) − 2 REFSPAAV[25]
$G_{Mg^{+2}:Va:Va:O^{-2}}$ = +NSPINEL + 2ISPINEL + 8GGAMMA + 2RT(6ln(6)-5ln(5)) + DGREC − 6* REFSPAAV[26]
$G_{Fe^{+2}:Mg^{+2}:Va:O^{-2}}$ = +NSPINEL + 2ISPINEL + 4RTln(2)-2REFSPAAV + 7GFE3O4 − GMGFE2O4 + DGMF[*]
$G_{Fe^{+3}:Mg^{+2}:Va:O^{-2}}$ = +2GMGFE2O4 − 7 GFE3O4 + BFE3O4 + 4RTln(2) − 2JMGFE2O4[*]
$G_{Mg^{+2}:Fe^{+2}:Va:O^{-2}}$ = +GMGFE2O4 + BFE3O4[*]
$G_{Mg^{+2}:Fe^{+3}:Va:O^{-2}}$ = +GMGFE2O4[*]
$G_{*:*:Fe^{+2}:O^{-2}} = G_{*:*:Va:O^{-2}}$ = +2GFE3O4 + DFE3O4 − BFE3O4[11]
$G_{*:*:Mg^{+2}:O^{-2}} = G_{*:*:Va:O^{-2}}$ = +2GFE3O4 + 8MSPINEL − 2 NSPINEL − 4ISPINEL − 4RTln(2) + 4REFSPAAV[26]
Magnetic properties (p = 0.28)
For compounds containing only Fe cations T_C = +848 and β = +44.54[11]
For compounds containing only Mg cations T_C = 0 and β = 0[26]
For compounds containing Fe + Mg cations T_C = +375 and β = 0[*]
${}^0\beta_{Fe^{+3}:Fe^{+3},Mg^{+2}:Va:O^{-2}}$ = −85[*]

* parameters assessed in this work

compared with the experimental data by Schenck and Pfaff.[71] The liquidus temperatures are scattered, but the values from Scheel et al.[74] are well reproduced.

Table 2 List of parameters in the Fe-Ca-S system for phases that have been assessed in this work

Liquid
G_{Ca} = GLIQCA[98]
G_{Fe} = GFELIQ[98]
G_S = GLIQSS[98]
$G_{Ca:S}$ = 2GLIQCA + 2GLIQSS-826244 + 97.30360T[*]
$G_{Fe:S}$ = 2GFELIQ + 2GLIQSS + 2GLIQFES[10]
$L_{Ca,Fe:Va}$ = 120705[2]
$L_{Ca:S,Va} = L_{Ca:O,Va}$[2] = 17331
$L_{Ca:S-2,S0}$ = 100000[*]
$L_{Ca,Fe:S}$ = −55000[*]
${}^0L_{Fe:S,Va}$ = 103758 − 46.3734T[10]
${}^1L_{Fe:S,Va}$ = −27530[10]
${}^0L_{Fe:S^{-2},S_0}$ = 96626 − 43.614T[10]
${}^1L_{Fe:S^{-2},S_0}$ = −145966 + 49.429T[10]
Alabandite
$G_{Ca:S}$ = GHSERSS + GHSERCA − 476000 + 57.22T[*]
$G_{Fe:S}$ = GHSERFE + GHSERSS + GFES + 5380 − 2.37T[23]
$L_{Ca,Fe:S}$ = 46000[*]

* parameters assessed in this work

Table 3 List of parameters in the Fe-Mg-S system for phases that have been assessed in this work

Liquid
G_{Fe} = GFELIQ[98]
G_{Mg} = GLIQMG[98]
G_S = GLIQSS[98]
$G_{Fe:S}$ = 2GFELIQ + 2GLIQSS + 2GLIQFES[10]
$G_{Mg:S}$ = 2GLIQMG + 2GLIQSS-619140 + 94.71262T
${}^0L_{Fe:S,Va}$ = 103758 − 46.3734T[10]
${}^1L_{Fe:S,Va}$ = −27530[10]
${}^0L_{Fe:S^{-2},S_0}$ = 96626 − 43.614T[10]
${}^1L_{Fe:S^{-2},S_0}$ = −145966 + 49.429T[10]
${}^0L_{Fe,Mg:Va}$ = 61343 + 1.5T[9]
${}^1L_{Fe,Mg:Va}$ = −2700[9]
$L_{Mg:S,Va} = L_{Mg:O,Va}$ = 182000 + 26.8T[*]
$L_{Fe,Mg:S}$ = 18000[*]
$L_{Mg:S^{-2},S_0}$ = 100000[*]
Alabandite
$G_{Fe:S}$ = GHSERFE + GHSERSS + GFES + 5380-2.37T[23]
$G_{Mg:S}$ = GHSERSS +GHSERMG + 351456 + 50.25T[*]
${}^0L_{Fe,Mg:S}$ = 8140[*]
${}^1L_{Fe,Mg:S}$ = 4900[*]

* parameters assessed in this work

FeO-Fe_2O_3-MgO. Philips and Muan[67] studied the isothermal section FeO-Fe_2O_3-MgO at temperatures from 1673 to 1873 K. Oxygen isobars in the FeO-Fe_2O_3-MgO ternary were measured by several authors[52,62,63,76] at various temperatures (1433 to 1673 K). Calculated isothermal sections of the FeO-Fe_2O_3-MgO phase diagram are shown in Fig. 7 for the temperatures 1433 and 1573 K with log(P_{O2}) isobars. The experimental data from Katsura and Kimura[52] as well as Speidel[62] are in reasonable agreement with the present assessment.

Table 4 List of functions used in the descriptions

Functions
GFELIQ (298.15 < T < 1811) = +GHSERFE + 12040.17 – 6.55843T 3.6751551E – 21T^7
GFELIQ (1811 < T < 6000) = −10839.7 + 291.302T – 46Tln(T)
GHSERFE (298.15 < T < 1811) = +1224.83 + 124.134T – 23.5143 Tln(T) – 0.00439752T^2 – 5.89269E – 08T^3 + 77358.5/T
GMGLIQ (298.15 < T < 923) = +GHSERMG + 8202.243 – 8.83693T 8.0176E – 20T^7
GMGLIQ (923 < T < 3000) = +GHSERMG + 8690.316 – 9.392158T 1.038192E + 28T^{-9}
GFEOLIQ = −137252 + 224.641T – 37.1815Tln(T)
GMGOLIQ (298.15 < T < 1700) = −549098.33 + 275.724634T 47.4817Tln(T) – 0.00232681*T^2 + 4.5043E – 08T^3 + 516900/T
GMGOLIQ (1700 < T < 2450) = −585159.646 + 506.06825T – 78.3772 Tln(T) + 0.0097344T^2 – 8.60338E – 07T^3 + 8591550/T
GMGOLIQ (2450 < T < 3100) = +9110429.75 – 42013.7634 T + 5298.548Tln(T) – 1.30122485T^2 + 5.8262601E – 05T^3 – 3.24037416 E + 09/T
GMGOLIQ (3100 < T < 5100) – 632664.468 + 589.239555T – 84Tln(T)
GWUS$T1T$E = −279318 + 252.848T – 46.12826ln$T$ln(T) – 0.0057402984 T^2
AWUS$T1T$E = −55384 + 27.888T
GMGOSOL (298.15 < T < 1700) = −549098.33 + 275.724634T 47.4817Tln(T) – 0.00232681T^2 + 4.5043E – 08T^3 + 516900/T
GMGOSOL (1700 < T < 2450) = −585159.646 + 506.06825T 78.3772Tln(T) + 0.0097344T^2 – 8.60338E – 07T^3 + 8591550/T
GMGOSOL (2450 < T < 3100) = +9110429.75 – 42013.7634 T + 5298.548Tln(T) – 1.30122485T^2 + 5.8262601E – 05T^3 – 3.24037416 E + 09/T
GMGOSOL (3100 < T < 5100) – 632664.468 + 589.239555T – 84Tln(T)
GFE3O4 = – 161731 + 144.873T – 24.9879Tln(T) – 0.0011952256 T^2 + 206520/T
BFE3O4 = 46826 – 27.266T
CFE3O4 = +120730 – 20.102T
DFE3O4 = +402520 – 30.529T
NSPINEL = +GMGOSOL + GCORUND – 27600 – 62T + 9ln(T)
ISPINEL = +NSPINEL + 51600 – 39T
MSPINEL = +GMGOSOL + 58000 – 18T
GGAMMA (298.15 < T < 600) = −1689977.34 + 469.458181T 70.5452Tln(T) – 0.070794T^2 + 1.491345E – 05T^3 + 981165/T
GGAMMA (600 < T < 1500) = −1708389.72 + 791.591946T – 121.754 Tln(T) – 0.0075467T^2 + 2.89573E – 07T^3 + 2222750/T
GGAMMA (1500 < T < 3000) = −1758861.74 + 1110.41976T 164.253Tln(T) + 0.00775305T^2 – 6.8247E – 07T^3 + 13162750/T
DGREC = +108000
REFSPAAV = 10.5NSPFEAL – 3.5GFE3O4 – 0.5BFE3O4 + 32900
GFE2O3 = −858683 + 827.946T – 137.0089Tln(T) + 1453810/T
GCORUND (298.15 < T < 600) = −1707351.3 + 448.021092*T 67.4804Tln(T) – 0.06747T^2 + 1.4205433E – 05T^3 + 938780/T
GCORUND (600 < T < 1500) = −1724886.06 + 754.856573*T 116.258Tln(T) – 0.0072257T^2 + 2.78532E – 07T^3 + 2120700/T
GCORUND (1500 < T < 3000) = −1772163.19 + 1053.4548*T 156.058Tln(T) + 0.00709105T^2 – 6.29402E – 07T^3 + 12366650/T
GMGFE2O4 = +GFE2O3 + GMGOSOL + 20100 + 13T
JMGFE2O4 = +52100
DGMF = +40000

Table 4 continued

Functions
GLIQCA = +5844.846 + 62.4838T – 16.3138Tln$T$ – 0.01110455T^2 133574/T
GHSERSS (298.15 < T < 368.3) = −5228.956 + 55.401762T – 11.007 Tln(T) – 0.026529T^2 + 7.754333E – 06T^3
GHSERSS (T < 368.3 < T < 1300) = −6513.769 + 94.676922T 17.941839Tln(T) – 0.010895125T^2 + 1.402558E – 06T^3 + 39910/T
GHSERCA (298.15 < T < 1115) = −4955.062 + 72.794266T 16.3138Tln(T) – 0.01110455T^2 – 133574/T
GHSERCA (1115 < T < 3000) = −107304.428 + 799.982066T 114.292247Tln(T) + 0.0237338147T^2 – 1.2438E – 06T^3 + 18245540/T
GHSERCA (3000 < T < 3001) = −3703.12 + 192.63995*T – 35Tln(T)
GLIQSS (298.15 < T < 388.36) = −4001.549 + 77.889686T – 15.504 Tln(T) – 0.018629T^2 – 2.4942E – 07T^3 – 113945/T
GLIQSS (T < 388.36 < T < 428.15) = −5285183.35 + 118449.585T 19762.47Tln(T) + 32.79275T^2 – 0.0102214167T^3 + 2.646735E + 08/T
GLIQSS (428.15E < T < 432.25) = −8174995.23 + 319914.078T 57607.3Tln(T) + 135.3045T^2 – .0529973333*T^3
GLIQSS (432.25 < T) = −219408.801 + 7758.83993T – 1371.85 Tln(T) + 2.845035T^2 – 0.001013803333T^3
GFES = −107518 – 18.19T + 1.78Tln(T)
GLIQFES = −104225 – 1.479T

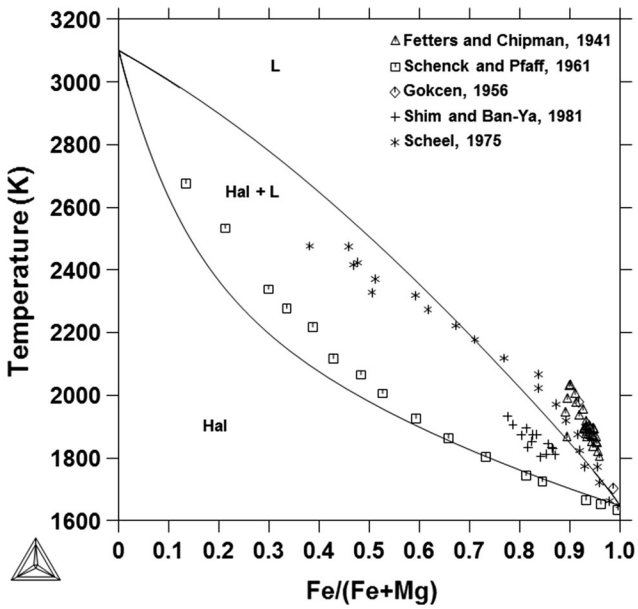

Fig. 6 Calculated pseudobinary MgO-"FeO" pseudobinary phase diagram assuming excess iron with experimental data[71-75]

FeO-Fe_2O_3-MgO Oxygen Partial Pressure. Activity measurements have been performed at various temperatures, at 1073 K,[63] 1173 K,[63,65] 1273 K,[56,58,63,65,66] 1373 K,[54,56,58,63-65] 1473 K,[63-65] 1573 K[54,62-64] and 1673 K.[61] Phase diagrams at various temperatures showing oxygen partial pressure versus composition are presented in Fig. 8. The calculated phase boundaries are within the experimental errors.

Calculated isothermal section in FeO-Fe_2O_3-MgO at 1873 K with experimental data on solubilities in the liquid[68] and stable phases[67] is shown in Fig. 9. The main discrepancy between the measurement and calculation is the MgO content at the liquidus, which is higher in the measurements than given by the calculation. But, as can be seen in Fig. 5, the reported liquidus composition within the spinel field is in disagreement with other measurements. The data from Schürmann and Kolm[68] was not used in the assessment procedure.

Activity of FeO. Activity measurements of FeO in halite were performed in two studies.[54,69] As can be seen in Fig. 10 the calculated activity is more ideal compared with the experimental results. This disagreement coincides with the disagreement of the cation distribution in halite as was shown in Fig. 3. However, it could also be a result of the fact that a "FeO"-MgO solution contains FeO_x rather than FeO. The disagreement is acceptable in order to obtain a good fit to other experimental results.

3.4 Fe-Ca-S

Despite its metallurgical importance, only limited experimental information is found for the Fe-Ca-S system and even the Ca-S system. Heat capacity of CaS at low temperature have been measured by Anderson.[77] In addition, the heat capacity has been calculated using DFT within GGA by Choutri et al.[78] The experimental heat capacity values are used to derive an entropy value, by numerical integration, which gives 57.22 J/K/mol at 294.9 K. The heat of formation has been reported by several authors.[79-83] In this study the compiled value

Fig. 8 Stable phases at oxygen partial pressure versus Mg/(Fe + Mg) at (a) 1173 K, (b) 1273, (c)1373, (d) 1473 and (e) 1573 with experimental data.[51,54,56,58-62,64-66] ✿ Woodhouse and White,[59] ⋇ Willshee and White,[60] ⋈ Wallace et al.,[61] ⋎ Srečec et al.,[51] ✯ Speidel,[62] ⏀ Hahn and Muan,[54] ⨯ Paladino,[63] ∗ Kang et al.,[64] + Maja and Abbattista,[58] ⧖ Schmalzried and Tretjakow,[65] ⏁ Wallet and Marion,[56] ⏃ Trinel-Dufour and Perrot[66]

−476 kJ/mol from Mills[83] is chosen since it is in agreement with most of the reported values. The melting point has been measured as 2798 K by Juza and Bünzen.[84] No heat of fusion data has been reported for CaS, which is also the case for MgS. For this reason, the melting entropy for MgO is used for both CaS and MgS. This value is 25 J/K/mol according to the Mg-O description by Hallstedt,[12] which is about the same as for the Ca-O description by Selleby and Sundman.[2] Except for pure CaS no data have been found for the Ca-S system. Therefore, parameters for the liquid from an assessment of the Ca-O system[2] are used as an approximation. This interaction parameter is rather low and thus no miscibility gap is formed on the metallic side of the phase diagram. This might be incorrect but given the lack of experimental data it is assumed that the Ca-O system is reasonably similar to the Ca-S system. In the Cu-S,[10] Fe-S[10] and Ni-S[85] systems there is a miscibility gap between sulphidic liquid and pure sulphur. Due to the high melting point of CaS there the existence of a miscibility gap in the CaS-S part of the system is uncertain. However, considering the larger ionic character, the immiscibility between CaS and S is likely higher than that with Fe, Cu and Ni. Thus the $L_{S\text{-}2,S}$ parameter is set so that a miscibility gap, which would be larger than the FeS-S miscibility gap if

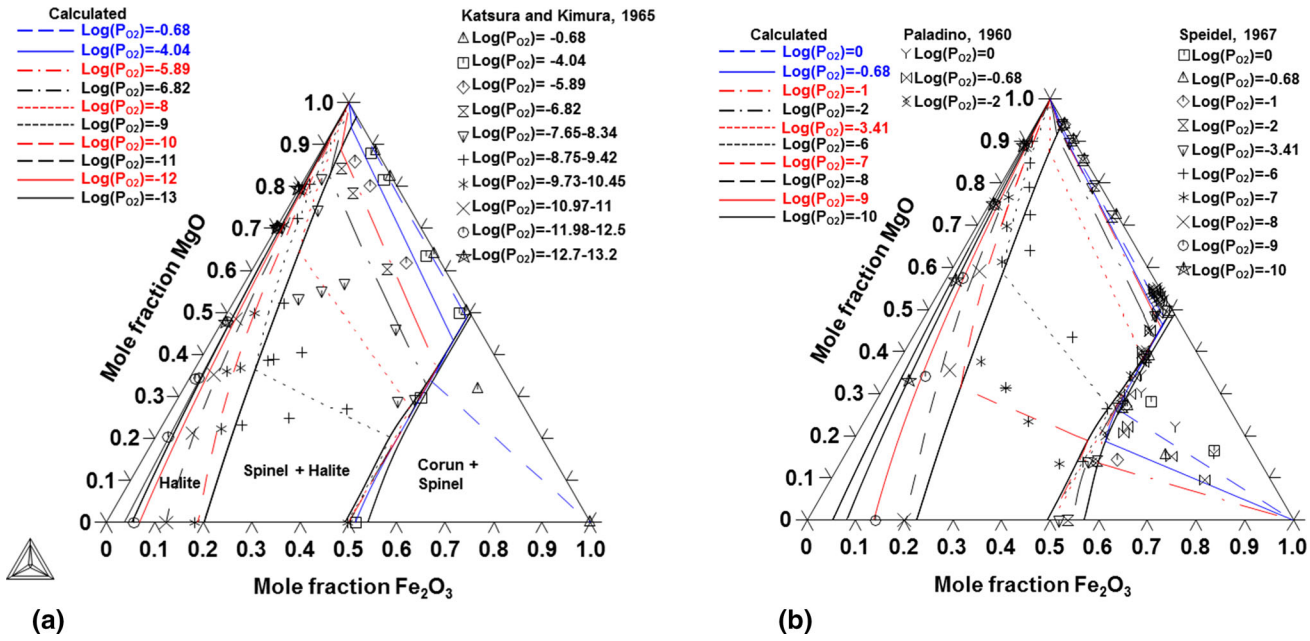

Fig. 7 (a) Calculated FeO-Fe_2O_3-MgO isothermal section at (a) 1433 K with experimental data[52] and (b) 1573 K with experimental data[62,63]

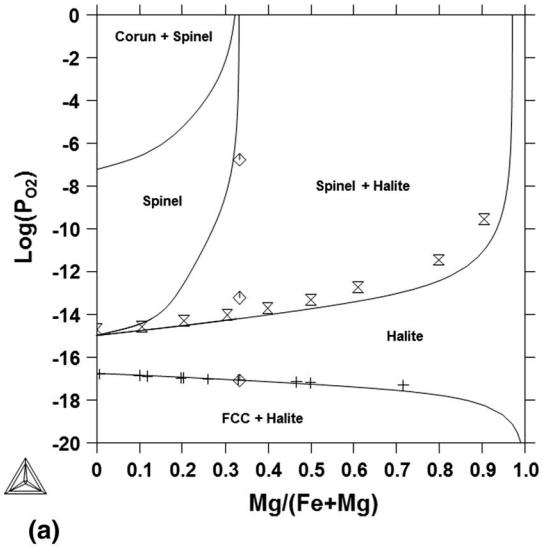
Corun + Spinel
Spinel
Spinel + Halite
Halite
FCC + Halite
Log(P$_{O2}$)
Mg/(Fe+Mg)
(a)

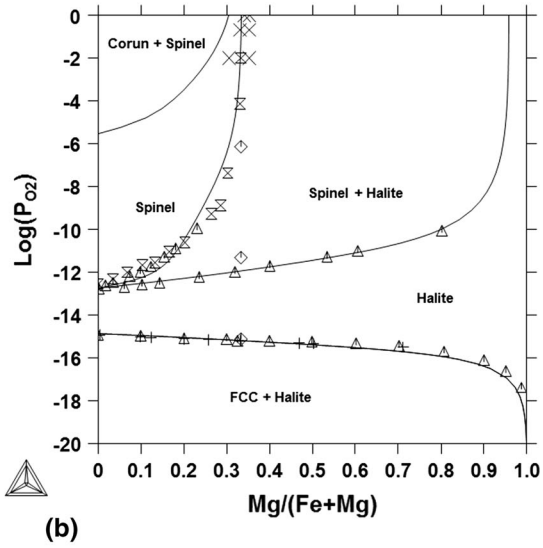
Corun + Spinel
Spinel
Spinel + Halite
Halite
FCC + Halite
Log(P$_{O2}$)
Mg/(Fe+Mg)
(b)

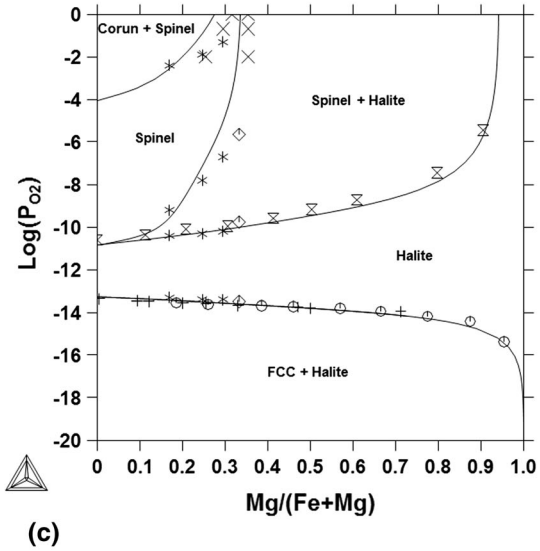
Corun + Spinel
Spinel
Spinel + Halite
Halite
FCC + Halite
Log(P$_{O2}$)
Mg/(Fe+Mg)
(c)

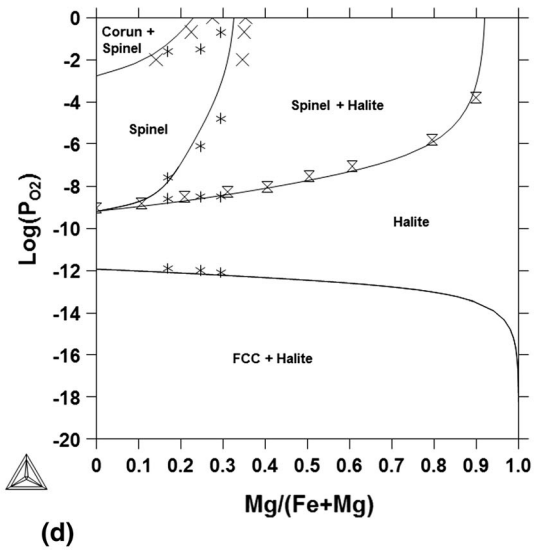
Corun +
Spinel
Spinel
Spinel + Halite
Halite
FCC + Halite
Log(P$_{O2}$)
Mg/(Fe+Mg)
(d)

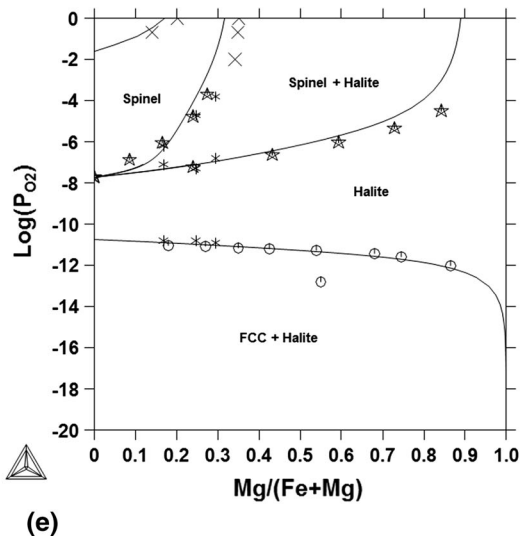
Spinel
Spinel + Halite
Halite
FCC + Halite
Log(P$_{O2}$)
Mg/(Fe+Mg)
(e)

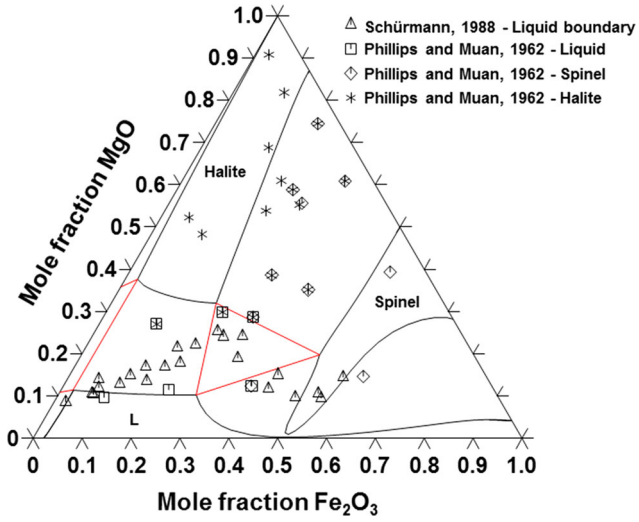

Fig. 9 Calculated Fe-Mg-O isothermal section at 1873 K together with experimental data[67,68]

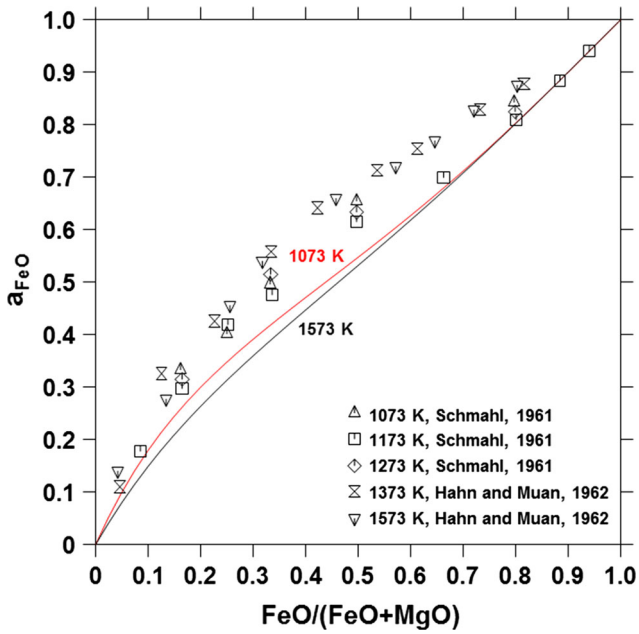

Fig. 10 Calculated FeO activity using halite as reference together with experimental data from[54,69]

CaS had the same melting point as FeS, is formed. The calculated Ca-S phase diagram is shown in Fig. 11.

The CaS-FeS binary section has been studied by Ref 30, 31, 86. These studies measured the solubility of FeS in CaS, which should be around 1 mass%, according to Vogel and Heumann,[30] but Huemann[86] later reported 2.1 mass% as the correct value. Skinner and Luce[31] reported the solubility to be less than 1 at.% FeS at 1273 K. In addition Vogel and Heumann[30] reported the eutectic point to be at 20 mass% CaS and 1393 K. Further on they report the data on two liquidus temperature close to the eutectic point.

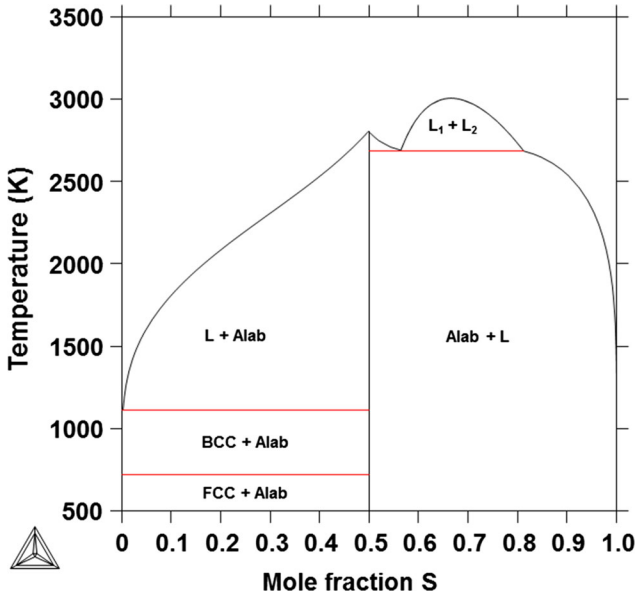

Fig. 11 The calculated Ca-S phase diagram with the gas phase suspended

However, as with the solubility of FeS in CaS, Heumann[86] later reported new values on the eutectic point, i.e. 12 mass% CaS and 1373 K. This study also presents new liquidus data close to the eutectic point and reports problems with sample purity in the earlier study. The study by Heumann[86] is chosen due to the higher sample purity. However, the shape of the liquidus curve rather than the eutectic temperature is believed to be most reliable, thus the eutectic temperature is set to 90 K lower than reported experimentally. It should also be emphasized that the study by Heumann[86] can be fitted using fewer interaction parameters than that of Vogel and Heumann,[30] which is an indication that the study by Heumann is more reliable. The description of [NaCl]-FeS (alabandite) is adopted from the Fe-Mn-S description.[23] The experimental data is compared to the calculated FeS-CaS pseudobinary section in Fig. 12.

The only ternary information that has been reported is phase diagram data for an isoplethal section at low calcium content as reported by Vogel and Heumann.[30] Their phase transition data is shown together with the calculated isoplethal section in Fig. 13. In the calculation, the bcc phase is ignored thus using the fcc phase to represent any solid iron phase. The reason for this is that Vogel and Heumann just report solid iron, and thus do not report bcc and fcc separately. The phase regions agree well with the experimental data but some phase transitions are missing in the experiments. Calculations predict a miscibility gap which has not been reported by Vogel and Heumann.[30] However, one could assume that the reported L/(L + CaS) phase boundary is in fact the miscibility gap. Using this assumption these experimental points show a reasonable agreement with the calculations. Given the uncertainties of the study by Vogel and Heumann[30] and because this isoplethal section is rather close to the accepted Fe-S binary

section it is decided not to set any parameter in the low-sulphur ternary section. The calculated isothermal section at 1873 K is shown in Fig. 14.

3.5 Fe-Mg-S

The experimental information concerning the Mg-S and Fe-Mg-S systems is limited. The heat capacity of MgS at low temperatures has been measured by Stull et al.[87] and has also been calculated using ab initio, in the same study as CaS.[78] The entropy is integrated numerically from the heat capacity which gives 50.25 J/K/mol at 298.15 K. There are some reports on the heat of formation.[79,83,88-90] Out of these, the compiled value given by Mills[83] is used since it agrees with most reported results. Since sulphur has weaker bonds to magnesium than oxygen it is also assumed that the melting point must be below that of MgO, i.e. 3073 K.[12] According to Tiede and Schleede[91] the melting point should be at least 2273 K. However, the only study[92] that reports a value of the MgS melting temperature states that it is 2264 K. This melting point is accepted as it is the only reported value and since it is very close the lower limit suggested by Tiede and Schleede.[91] As in the case of CaS the melting entropy of MgO[12] is used for MgS. Except for MgS, no experimental data has been reported for the Mg-S binary. The liquid interaction parameters from the Mg-O binary description[12] are used to model the Mg-MgS side. In contrast to the Ca-S system this results in a really large miscibility gap in the metallic side of the Mg-S phase diagram, which is due to the different oxygen description used as approximations. The immiscibility might be too large considering that oxygen has a higher electronegativity than sulphur but it is a reasonable assumption considering the lack of experimental data. As in the case of Ca-S the $L_{S-2,S}$ parameter in the liquid should be set to a rather large value. Estimating the same value as in the Ca-S system a liquid miscibility gap is formed at high sulphur contents due to the lower melting point of MgS, as can be seen in Fig. 15.

The solid phases in the FeS-MgS system have been studied by Skinner and Luce[31] and Andreev et al.[92] The calculated FeS-MgS pseudobinary is shown in Fig. 16 together with experimental information. It is also studied in McCammon et al.[93] No data has been found for the Fe-

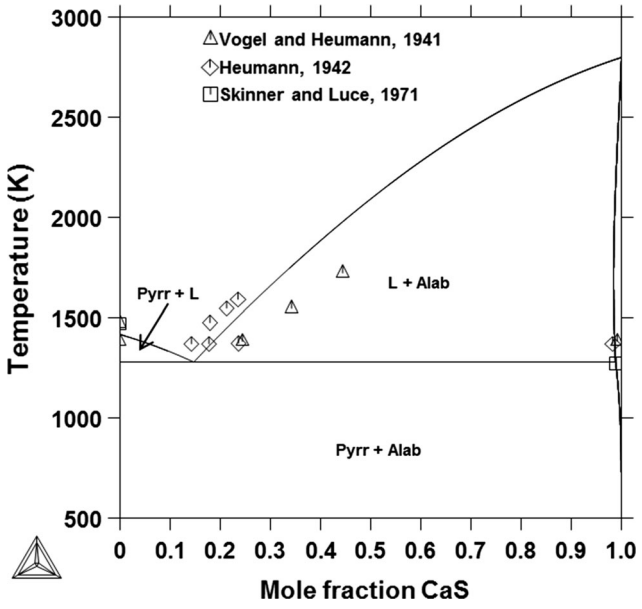

Fig. 12 The calculated FeS-CaS pseudobinary phase diagram with experimental data from[30,31,86]

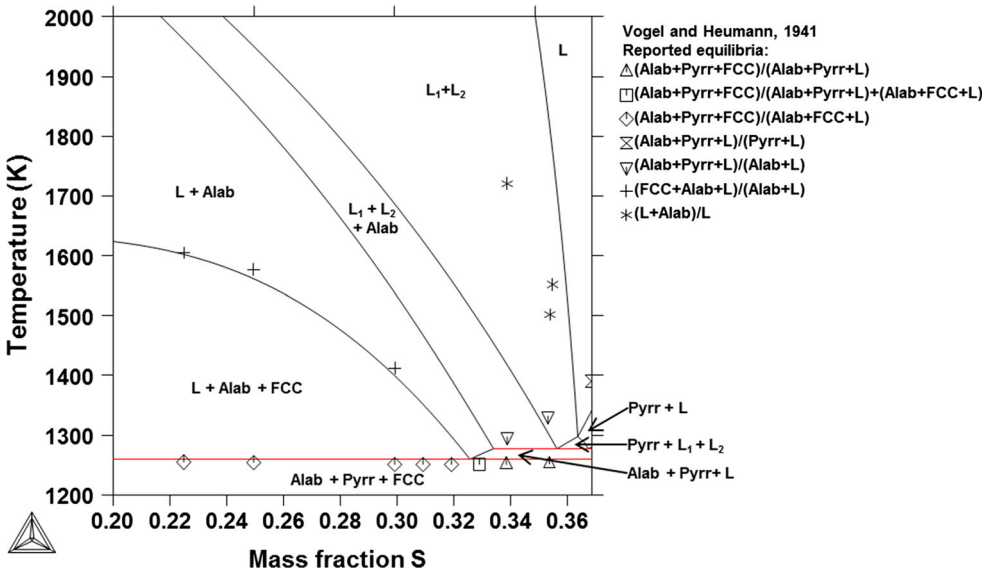

Fig. 13 The calculated isoplethal section at the mass ratio Ca:Fe = 0.07 with experimental phase boundary data from,[30] with gas and bcc suspended. Note that the experimental study does not report any liquid miscibility gap. The phases were named CaS (alab), FeS (pyrr), S (L) and Fe (FCC) in their publication

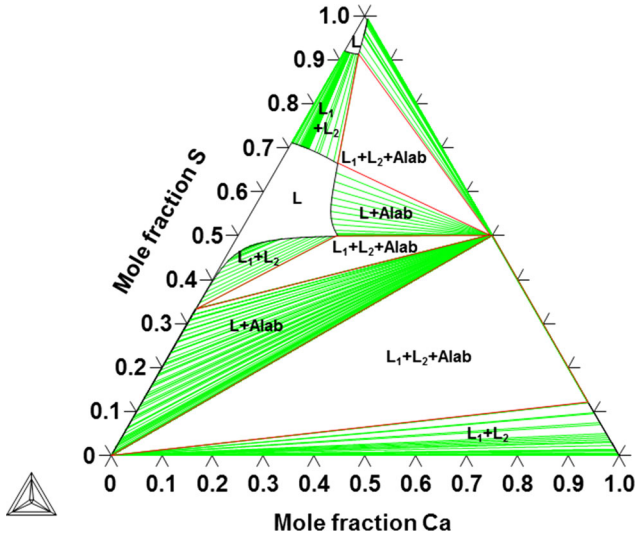

Fig. 14 The calculated Fe-Ca-S isothermal section at 1873 K with the gas phase suspended

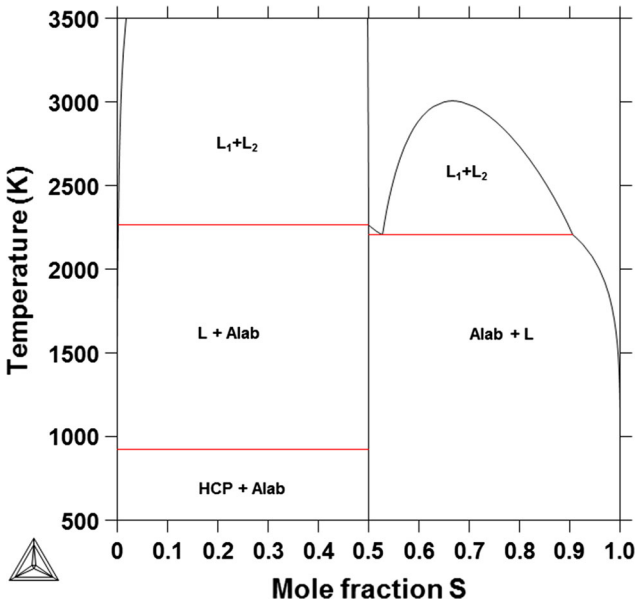

Fig. 15 The calculated Mg-S phase diagram with the gas phase suspended

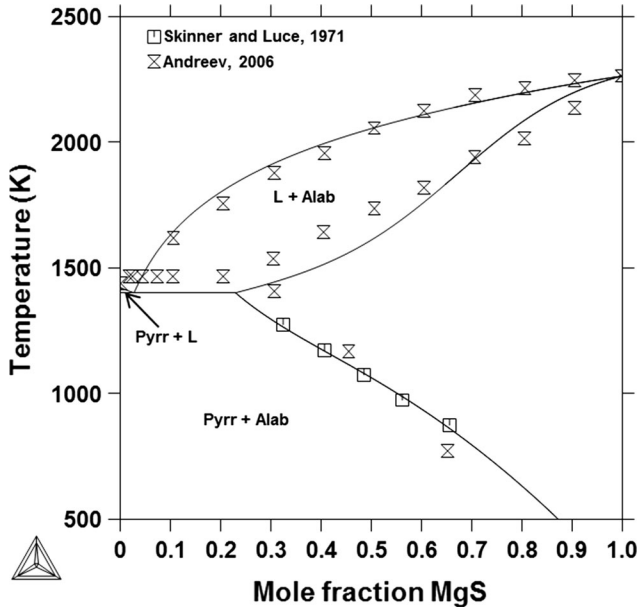

Fig. 16 The calculated FeS-MgS pseudobinary phase diagram with experimental data from [31,92]

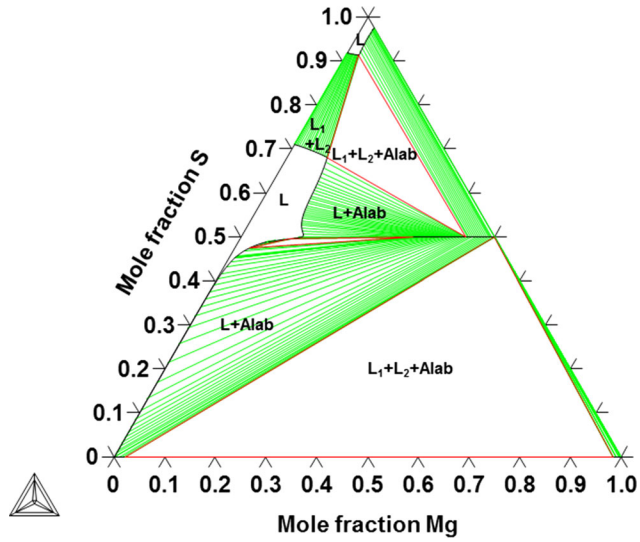

Fig. 17 The calculated Fe-Mg-S isothermal section at 1873 K with gas phase suspended

Mg-S ternary section. In Fig. 17 the isothermal section of the Fe-Mg-S system at 1873 K is presented.

3.6 Similarities Between the Systems

As mentioned throughout the paper the systems Fe-Ca-O, Fe-Ca-S, Fe-Mg-O and Fe-Mg-S are similar from a chemical point of view. A main difference is the fact that sulphur has a lower electronegativity than oxygen. This causes the melting point of the sulphides to be somewhat lower than their oxide counterparts. Additionally, given that sulphides are less ionic than oxides the mutual solubility between the solid sulphide and solid oxides is very low. Another difference is the ionic radius of calcium and magnesium. Since magnesium has a similar ionic radius as iron this means that [NaCl]-MgS can dissolve high amount of [NaCl]-FeS, as was shown in Fig. 16, and likewise that [NaCl]-FeO and [NaCl]-MgO have complete mutual solubility. In the case of CaS and CaO this is however not the case since the calcium ion is significantly larger than the iron(II) ion. It should also be mentioned that for this reason CaS and MgS[31] and CaO and MgO[94,95] have large

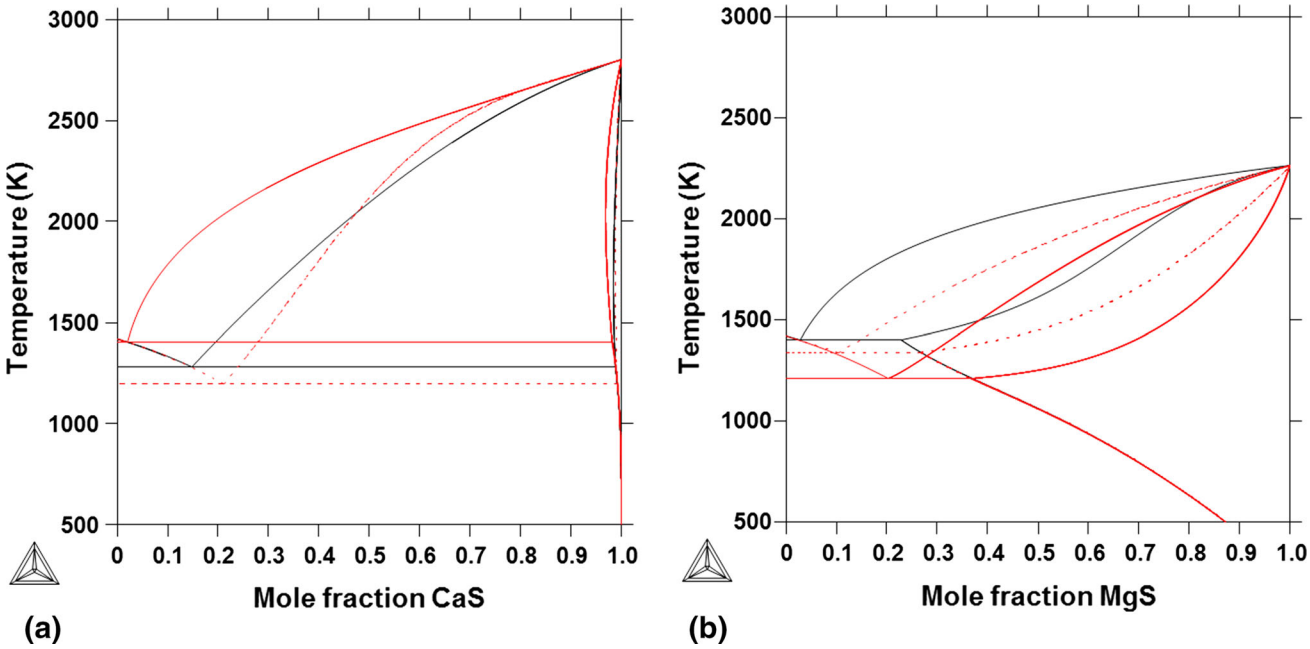

Fig. 18 Pseudobinaries calculated with corresponding oxide and sulphide liquid parameters, (a) FeS-CaS with its normal parameters (black) as well as FeO-CaO (dotted red) and FeS-MgS (red) parameters and (b) FeS-MgS with its normal parameters (black) as well as FeO-MgO (dotted red) and FeS-CaS (red) parameters (Color figure online)

miscibility gaps. It is reasonable to assume that the ionic radius has less influence in the liquid phase. Given this and that liquid sulphides behaves strongly ionic it is reasonable to assume that all these liquids behave similarly. This assumption is used considering the entropy of fusion, which is set equal for CaO, CaS, MgO and MgS. Additionally the liquid parameters for Ca-S and Mg-S have been set using their oxygen counterparts due to lacking experimental information. To investigate this similarity the sulphide pseudobinary phase diagrams are calculated using liquid interaction parameters from their corresponding systems, sulphide and oxide, as is shown in Fig. 18. In these calculations all parameters are taken from this work except the FeO-CaO parameters which are taken from Selleby and Sundman.[2] As can be seen, the graphs for the sulphide systems are reproduced rather well by their corresponding oxide systems. It is worth to mention that even selenides and sulphides can be really similar as is shown for the CaS-MnS and CaSe-MnSe systems.[96] Approximating parameters in an alkaline earth metal sulphide system by using a similar alkaline earth metal sulphide, is however not as good approximation as using the corresponding oxide systems.

4. Conclusions

Thermodynamic descriptions of the Fe-Mg-O, Fe-Ca-S and Fe-Mg-S systems have been presented. The description of the Fe-Mg-O system reproduces both thermochemical and phase diagram data well. Despite the fact the Fe-Ca-S and Fe-Mg-S descriptions are largely based on assumptions, they can probably predict the unknown parts of the phase diagrams reasonably well. The reason for this is that most assumptions are based on the fact that Ca and Mg as well as O and S are quite similar from a chemical point of view. However, it is still desirable to fill this knowledge gap with experimental studies. Since both oxygen and sulphur are of importance for steelmaking a natural next step would be to combine these systems.

Acknowledgments

The present Project, Compass, is funded by KTH Royal Institute of Technology, Outokumpu Stainless Foundation, Ovako, SSAB EMEA and Thermo-Calc Software. Dr Huahai Mao is acknowledged for many useful discussions.

References

1. M. Hillert, M. Selleby, and B. Sundman, An Assessment of the Ca-Fe-O System, *Metall. Mater. Trans. A*, 1991, **21**, p 2759-2776
2. M. Selleby and B. Sundman, A Reassessment of the Ca-Fe-O System, *CALPHAD*, 1996, **20**, p 381-392
3. M. Hillert, B.O. Jansson, B.O. Sundman, and J. Ågren, A Two-Sublattice Model for Molten Solutions with Different Tendency for Ionization, *Metall. Trans. A*, 1985, **16**, p 261-266
4. B. Sundman, Modification of the Two-Sublattice Model for Liquids, *CALPHAD*, 1991, **15**, p 109-119
5. O. Fabrichnaya, The Assessment of Thermodynamic Parameters for Solid Phases in the Fe-Mg-O and Fe-Mg-Si-O Systems, *CALPHAD*, 1998, **22**, p 85-125

6. I.H. Jung, S.A. Decterov, and A.D. Pelton, Critical Thermodynamic Evaluation and Optimization of the Fe-Mg-O System, *J. Phys. Chem. Solids*, 2004, **65**, p 1683-1695
7. A.D. Pelton, S.A. Degterov, G. Eriksson, C. Robelin, and Y. Dessureault, The Modified Quasichemical Model I—Binary Solutions, *Metall. Mater. Trans. B*, 2000, **31**, p 651-659
8. D. Lindberg and P. Chartrand, Thermodynamic Evaluation and Optimization of the (Ca + C+O + S) System, *J. Chem. Thermodyn.*, 2009, **41**, p 1111-1124
9. J. Tibballs, System Fe-Mg, *COST 507 Thermochem. Database Light Metal Alloys*, Vol 2, I. Ansara, A.T. Dinsdale, and M. Rand, Ed., European C, Brussels, 1998, p 195-196
10. B. Lee, B. Sundman, S. Il Kim, and K. Chin, Thermodynamic Calculations on the Stability of Cu2S in Low Carbon Steels, *ISIJ Int.*, 2007, **47**, p 163-171
11. B. Sundman, An Assessment of the Fe-O System, *J. Phase Equilib.*, 1991, **12**, p 127-140
12. B. Hallstedt, The Magnesium-Oxygen System, *Calphad.*, 1993, **17**, p 281-286
13. L. Kaufman and H. Bernstein, *Computer Calculation of Phase Diagrams*, Academic Press, New York, 1970
14. M. Hillert and L.-I. Staffansson, The Regular Solution Model for Stoichiometric Phases and Ionic Melts, *Acta Chem. Scand.*, 1970, **24**, p 3618-3626
15. M. Hillert, The Compound Energy Formalism, *J. Alloys Compd.*, 2001, **320**, p 161-176
16. S. Holgersson, Die Struktur der Sulfide von Mg, Ca, Sr und Ba, *Z. Für Anorg. Und Allg. Chem.*, 1923, **126**, p 179-182
17. C.N.R. Rao and K.P.R. Pisharody, Transition Metal Sulfides, *Progess Solid State Chem.*, 1974, **10**, p 207-270
18. H.C. Chao, Y.E. Smith, and L.H. van Vlack, The MnO-MnS Phase Diagram, *Trans. Metall. Soc. AIME.*, 1963, **227**, p 796-797
19. L. Kjellqvist, M. Selleby, and B. Sundman, Thermodynamic Modelling of the Cr-Fe-Ni-O System, *CALPHAD*, 2008, **32**, p 577-592
20. L. Kjellqvist and M. Selleby, Thermodynamic Assessment of the Mn-Ni-O System, *Int. J. Mater. Res.*, 2010, **101**, p 1222-1231
21. L. Kjellqvist and M. Selleby, Thermodynamic Assessment of the Fe-Mn-O System, *J. Phase Equilib. Diffus.*, 2010, **31**, p 113-134
22. H. Mao, M. Hillert, M. Selleby, and B. Sundman, Thermodynamic Assessment of the CaO-Al2O3-SiO2 System, *J. Am. Ceram. Soc.*, 2006, **89**, p 298-308
23. D. Dilner, H. Mao, and M. Selleby, Thermodynamic Assessment of the Mn-S and Fe-Mn-S Systems, *CALPHAD*, 2015, **48**, p 95-105
24. A.N. Grundy, B. Hallstedt, and L.J. Gauckler, Assessment of the Mn-O System, *J. Phase Equilib.*, 2003, **24**, p 21-39
25. H. Rau, Defect Energetics and Range of Homogeneity of α-MnS, *J. Phys. Chem. Solids*, 1978, **39**, p 339-343
26. B. Hallstedt, Thermodynamic Assessment of the System MgO-Al203, *J. Am. Ceram. Soc.*, 1992, **75**, p 1497-1507
27. M. Hillert, L. Kjellqvist, H. Mao, M. Selleby, and B. Sundman, Parameters in the Compound Energy Formalism for Ionic Systems, *CALPHAD*, 2009, **33**, p 227-232
28. Inden, Determination of Chemical and Magnetic Interchange Energies in BCC Alloys—I. General Treatment, *Ze. Für Met.*, 1975, **66**, p 577-582
29. M. Hillert and M. Jarl, A Model for Alloying in Ferromagnetic Metals, *CALPHAD*, 1978, **2**, p 227-238
30. R. Vogel and T. Heumann, Das System Eisen-Eisensulfid-Kalziumsulfid, *Arch. Für Das Eisenhüttenwes*, 1941, **15**, p 195-199
31. B.J. Skinner and F.D. Luce, Solid Solution of the Type (Ca, Mg, Mn, Fe)S and Their Use as Geothermometers for the Enstatite Chondrites, *Am. Miner.*, 1971, **56**, p 1269-1296
32. J.-O. Andersson, T. Helander, L. Höglund, P. Shi, and B. Sundman, THERMO-CALC & DICTRA, Computational Tools For Materials Science, *CALPHAD*, 2002, **26**, p 273-312
33. E.G. King, Heat Capacities at Low Temperatures and Entropies at 298.16 K of Calcium and Magnesium Ferrites, *J. Am. Chem. Soc.*, 1954, **76**, p 5849-5850
34. L.A. Reznitskii, K.G. Khomyakov, N.G. Korzhukov, and S.E. Orel, Calorimeter for Determining the True Heat Capacity of Ferrites from 300 to 1000 K, *Fiz. Khim.*, 1969, **43**(1969), p 2165-2169
35. K.R. Bonnickson, High Temperature Heat Contents of Calcium and Magnesium Ferrites, *J. Am. Chem. Soc.*, 1954, **76**, p 1480-1482
36. J.A. Shearer and O.J. Kleppa, The Enthalpies of Formation of MgAl2O4, MgSiO3, Mg2SiO4 and Al2SiO5 by Oxide Melt Solution Calorimetry, *J. Inorg. Nucl. Chem.*, 1973, **35**, p 1073-1078
37. M.F. Koehler, B. Barany, K.K. Kelley, *Heats and Free Energies of Formation of Ferrites and Aluminates of Calcium, Magnesium, Sodium, Lithium*, Report of Investigations 5711, Washington, 1961
38. J.D. Tretjakow and H. Schmalzried, Zur Thermodynamik von Spinellphasen, *Berichte Der Bunsengesellschaft*, 1965, **69**, p 396-402
39. A. Navrotsky, Cation-Distribution Energetics and Heats of Mixing in MgFe2O4-MgAl2O4, ZnFe2O4-ZnAl2O4, and NiAl2O4-ZnAl2O4 Spinels: Study by High-Temperature Calorimetry, *Am. Miner.*, 1986, **71**, p 1160-1169
40. A. Navrotsky and O.J. Kleppa, Thermodynamics of Formation of Simple Spinels, *J. Inorg. Nucl. Chem.*, 1968, **30**, p 479-498
41. L. Wang, H. Zhou, Y. Hong, and G.M. Kale, Electrochemical Determination of Gibbs Free Energy of Magnesium Ferrite, *J. Univ. Sci. Technol. Beijing*, 2007, **14**, p 361-364
42. H. O'Neill, H. Annersten, D. Virgo, Powder XRD Structural Refinements and Miissbauer Spectroscopy, 1992, **77**, p 3-4
43. R.L. Mozzi and A.E. Paladino, Cation Distributions in Nonstoichiometric Magnesium Ferrite, *J. Chem. Phys.*, 1963, **39**, p 435-439
44. C.J. Kriessman and S.E. Harrison, Cation Distributions in Ferrospinels. Magnesium-Manganese Ferrites, *Phys. Rev.*, 1956, **103**, p 857-860
45. D.J. Epstein and B. Frackiewicz, Some Properties of Quenched Magnesium Ferrites, *J. Appl. Phys.*, 1958, **29**, p 376-377
46. J.G. Faller and C.E. Birchenall, The Temperature Dependence of Ordering in Magnesium Ferrite, *J. Appl. Crystallogr.*, 1970, **3**, p 496-503
47. J.-C. Tellier, Sur la substitution dans le ferrite de magnésium des ions ferriques par des ions trivalents, tétravalents et pentavalents, *Rev. Chim. Minérale.*, 1967, **4**, p 325-365
48. R. Pauthenet and L. Bochirol, Aimantation Spontanée des Ferrites, *Le J. Phys. Le Radium.*, 1954, **12**, p 249-251
49. A. Trestman-Matts, S.E. Dorris, and T.O. Mason, Thermoelectric Determination of Cation Distributions in Iron Oxide-Iron Magnesium Oxide (Fe3O4-MgFe2O4), *J. Am. Ceram. Soc.*, 1984, **67**, p 69-74
50. J. Nell, B.J. Wood, and T.O. Mason, High-Temperature Cation Distributions in Fe3O4-MgAl2O4- MgFe2O4-FeAl2O4 Spinels from Thermopower and Conductivity Measurements, *Am. Miner.*, 1989, **74**, p 339-351
51. I. Srečec, A. Ender, E. Woermann, W. Gans, E. Jacobsson, G. Eriksson, et al., Activity-Composition Relations of the Magnesiowüstite Solid Solution Series in Equilibrium with Metallic Iron in the Temperature Range 1050-1400 K, *Phys. Chem. Miner.*, 1987, **14**, p 492-498

52. T. Katsura and S. Kimura, Equilibria in the System FeO-Fe2O3-MgO at 1160 °C, *Bull. Chem. Soc. Jpn.*, 1965, **38**, p 1664-1670
53. B. Simons, Composition-Lattice Parameter Relationship of the Magnesio-Wüstite Solid Solution Series, Carnegie Inst. Washington, Yearb, 1980, p 376-380
54. W.C. Hahn and A. Muan, Activity Measurements in Oxide Solid Solutions: The System "FeO"-MgO in the Temperature Interval 1100 to 1300 °C, *Trans. Metall. Soc. AIME*, 1962, **224**, p 416-420
55. N.M. Wiser and B.J. Wood, Experimental Determination of Activities in Fe-Mg Olivine at 1400 K, *Contrib. Mineral. Petrol.*, 1991, **108**, p 146-153
56. N. Wallet and M.F. Marion, Sur la réduction progressive des ferrites de magnésium et de nickel, *Académie Des Sci.*, 1963, **256**, p 1790-1796
57. P. Saha and G.M. Biggar, An Investigation of Magnesio-Wüstite as a Calibrant of Oxygen Fugacity, *Indian J. Earth Sci.*, 1974, **1**, p 131-140
58. M. Maja and F. Abbattista, Caratteristiche termodinamiche del sistema Magnesia-Wustite, *La Metall. Ital.*, 1973, **10**, p 565-570
59. D. Woodhouse and J. White, Phase Relationships of Iron-Oxide-Containing Spinels, *Trans. J. Br. Ceram. Soc.*, 1954, **53**, p 422-459
60. J.C. Willshee and J. White, An Investigation of Equilibrium Relationships in the System MgO-FeO-Fe_2O_3 up to 1750 8C in Air, *Trans. Br. Ceram. Soc.*, 1967, **66**, p 541-555
61. M. Wallace, S. Sun, S. Jahanshahi, Thermodynamic Constraints on Slag-Refractory Interaction: The Effect of Oxygen Potential on Spinel and Wustite Stability in the MgO-FeO-Fe2O3 System, *6th AusIMM Extractive Metallurgy Conference, Brisbane*, 1994, p 37-40
62. D. Speidel, Phase Equilibria in the System MgO-FeO-Fe2O3: The 1300 C Isothermal Section and Extrapolations to Other Temperatures, *J. Am. Ceram. Soc.*, 1967, **50**, p 243-248
63. A.E. Paladino, Phase Equilibria in the Ferrite Region of the System FeO-MgO-Fe2O3, *J. Am. Ceram. Soc.*, 1960, **43**, p 183-191
64. S.-H. Kang, S.-H. Chang, and H.-I. Yoo, Phase Stability of the System Mg-Fe-O, *J. Solid State Chem.*, 2000, **149**, p 33-40
65. H. Schmalzried and J.D. Tretjakow, Fehlordnung in Ferriten, *Berichte Der Bunsengesellschaft*, 1966, **70**, p 180-189
66. M.C. Trinel-Dufour and P. Perrot, Étude thermodynamique des solutions solides dans le système Fe-Mg-O, *Ann. Chim.*, 1977, **2**, p 309-318
67. B. Phillips and A. Muan, Phase Equilibria in the System MgO-FeO- Fe2O3 in Temperature Range 1400° to 1800° C, *J. Am. Ceram. Soc.*, 1962, **48**, p 588-591
68. E. Schürmann and I. Kolm, Einfluß der Fe2O3-Gehalte in Frischschlacken auf die MgO-Löslichkeit bei verschiedenen Sauerstoffpartialdrücken des Schlacke-Gas-Gleichgewichtes, *Steel Res.*, 1988, **59**, p 185-191
69. N. Schmahl, B. Frisch, and G. Stock, Gleichgewichtsuntersuchungen an Magnesiowustiten und Magnesioferriten, *Arch. Eisenhuttenwes.*, 1961, **32**, p 297-302
70. B. Phillips, S. Somiya, and A. Muan, Melting Relations of Magnesium Oxide-Iron Oxide Mixtures in Air, *J. Am. Ceram. Soc.*, 1961, **44**, p 167-169
71. H. Schenck and W. Pfaff, Das System Eisen(II)-oxyd-Magnesiumoxyd und seine Verteilungs-gleichgewichte mit flussigem Eisen bei 1520 bis 1750 C, *Arch. Eisenhuttenwes.*, 1961, **32**, p 741-751
72. K.L. Fetters and J. Chipman, Equilibria of Liquid Iron and Slags of the System CaO-MgO-FeO-SiO2, *Trans. Metall. Soc. AIME*, 1941, **145**, p 95-112
73. N.A. Gokcen, Equilibria in Reactions of Hydrogen, and Carbon Monoxide with Dissolved Oxygen in Liquid Iron; Equilibrium in Reduction of Ferrous Oxide with Hydrogen, and Solubility of Oxygen in Liquid Iron, *J. Met.*, 1956, **8**, p 1558-1567
74. R. Scheel, Gleichgewichte im System CaO-MgO-FeOn bei Gegenwert von metallischem Eisen, Sprechsaal Für Keramik, *Glas. Email*, 1975, **108**, p 685-686
75. J. Shim and S. Ban-ya, The Solubility of Magnesia and Ferric-Ferrous Equilibrium in Liquid FetO-SiO2-CaO-MgO Slags, 1981
76. J. Brynestad and H. Flood, The Redox Equilibrium in Wüstite and Solid Solutions of Wüstite and Magnesium Oxide, *Z. Für Elektrochem.*, 1958, **62**, p 953-958
77. C.T. Anderson, The Heat Capacities at Low Temperatures of Manganese Sulfide, Ferrous Sulfide and Calcium Sulfide, *J. Am. Chem. Soc.*, 1931, **53**, p 476-483
78. H. Choutri, M.A. Ghebouli, and N. Bouarissa, Lattice Dynamics and Thermal Properties of $Ca_xMg_{1-x}S$ Ternary Alloys, *Comput. Mater. Sci.*, 2013, **69**, p 148-152
79. H. von Wartenberg, Die Bildungswärme von Beryllium, Magnesium und Calciumsulfid, *Z. Fur Anorg. Chem.*, 1943, **252**, p 136-143
80. T. Rosenqvist, A Thermodynamic Study of the Reaction $CaS + H_2O = CaO + H_2S$ And the Desulphurization of Liquid Metal with Lime, *J. Met.*, 1951, **3**, p 535-540
81. L.F. Sander and G.W. Healy, On the Transformation of CaO to CaS at 1400 to 1650 °C, *Trans. Metall. Soc. AIME*, 1968, **242**, p 1039-1042
82. T. Uno, One Experiment on the Desulpurizing Action Lime, *Tetsu Hagane*, 1951, **37**, p 14-17
83. K.C. Mills, *Thermodynamic Data for Inorganic Sulphides*, Selenides and Tellurides, Wiltshire, 1974
84. R. Juza and K. Bünzen, Untersuchungen über das System Calciumcarbid/Calciumsulfid, *Z. Für Phys. Chem. Neue Folge*, 1958, **17**, p 82-99
85. P. Waldner and A.D. Pelton, Thermodynamic Modeling of the Ni-S system, *Z. Für Met.*, 2004, **95**, p 672-681
86. T. Heumann, Die Löslichkeit von Eisensulfid in Kalzium bei der eutektischen Temperatur, *Arch. Für Das Eisenhüttenwes.*, 1942, **15**, p 557-558
87. D.R. Stull, D.L. Hildenbrand, F.L. Oetting, and G.C. Sinke, Low Temperature Heat Capacities of 15 Inorganic Compounds, *J. Chem. Eng. Data*, 1970, **15**, p 52-56
88. A.F. Kaputinsky and J.A. Korshunov, A Direct Determination of the Heats of Formation of Sulphides (Ferrous, Cadmium, Zinc, Magnesium and Manganese Sulphides), *Acta Physicochim.*, 1939, **10**, p 259-272
89. E.W. Dewing and F.D. Richardson, The Thermodynamics of the Conversion of Magnesium and Manganese Oxides to Sulphides, *J. Iron Steel Inst.*, 1960, **195**, p 56-58
90. W. Curlock and M.L. Pidgeon, Determination of the Standard Free Energies of Formation of Zinc Sulfide and Magnesium Sulfide, *Trans. Metall. Soc. AIME*, 1958, **212**, p 671-676
91. E. Tiede and A. Schleede, Das Schmelzen der Sulfide von Zink, Cadmium und Quecksilber, *Berichte Der Dtsch. Chem. Gesellschaft.*, 1920, **53**, p 1717-1721
92. O.V. Andreev, A.V. Solov'eva, and T.M. Burkhanova, MgS-FeS Phase Diagram, *Russ. J. Inorg. Chem.*, 2006, **51**, p 1826-1828
93. C.A. McCammon, I. Jackson, A.E. Ringwood, and J.D. Cashion, The Binary Systems FeS-MgS and FeS-MnS: Mössbauer Spectroscopy of the B1 Solid Solutions and High-Pressure Phase Equilibria, *Phys. Chem. Miner.*, 1984, **11**(4), p 182-193

94. M. Hillert and X. Wang, Thermodynamic Calculation of the CaO-MgO System, *CALPHAD*, 1989, **13**, p 267-271
95. R.C. Doman, J.B. Barr, R.N. Mcnally, and A.M. Alper, Phase Equilibria in the System CaO-MgO, *J. Am. Ceram. Soc.*, 1963, **46**, p 313-316
96. C.-H. Leung and L.H. van Vlack, Solubility Limits in Binary (Ca, Mn) Chalcogenides, *J. Am. Ceram. Soc.*, 1979, **62**, p 613-616
97. H.S. Roberts and H.E. Merwin, The System MgO-FeO-Fe2O3 in Air at One Atmosphere, *Am. J. Sci.*, 1931, **21**, p 145-157
98. A.T. Dinsdale, SGTE Data for Pure Elements, *CALPHAD*, 1991, **15**, p 317-425
99. A.T. Dinsdale, Private Communication, Liquid and Solid Al_2O_3, CaO, MgO, (n.d.)